Electronic Supplementary Information

Uncovering Elusive Ultrafast Charge Transfer-Driven Structural Changes in 4,4′-bis(9-carbazol-9-yl)-1,1′-biphenyl, a Paradigmatic Molecular Triad

Jungkweon Choi,[a,b,+] Donghwan Im,[a,b,+] Jeong Hoon Lee,[a,b] Alekos Segalina,[a,b] and Hyotcherl Ihee[a,b,*]

[a] Department of Chemistry, Korea Advanced Institute of Science and Technology (KAIST), Daejeon 34141, Republic of Korea

[b] Center for Advanced Reaction Dynamics (CARD), Institute for Basic Science (IBS), Daejeon 34141, Republic of Korea

+ Both authors contributed equally to this work.

* Corresponding author: Hyotcherl Ihee

Lippert-Mataga plot

From the emission spectra measured in different polarizability conditions, we calculated the values of the difference of dipole moment between the initial and final states ($\Delta\mu = \mu_f - \mu_i$) of CBP using the Lippert-Mataga equation, shown below:

$$\tilde{v}_{stokes} = \frac{2(\Delta\mu)^2}{hca^3}\Delta f + C$$

Here, h is the Planck constant and c is the speed of light. According to this equation, the Stokes shift exhibits a linear dependence on the orientation polarizability, Δf, defined by the following expression:

$$\Delta f = \frac{\epsilon - 1}{2\epsilon + 1} + \frac{n^2 - 1}{2n^2 + 1}$$

where ε is the dielectric constant and n is the refractive index of the solvent. The parameter a represents the Onsager radius and is defined as: $a^3 = \frac{3V}{4\pi}$

Here, V is the volume of the solvent cavity for one molecule. In our calculations, as the shape of the molecule deviates from sphere shape, the Onsager radius of each molecule was determined from molecular volume calculations performed at the CAM-B3LYP/6-31G(d,p) level of theory, yielding values of 6.31 Å.

Table S1 Calculated vibrational frequencies and corresponding normal mode motions for four key vibrational modes at the minimum geometry of the S_1 state. Note that "o.o.p." refers to out-of-plane vibrational modes involving hydrogen atoms within each moiety

	frequency (cm^{-1})	motion
ν_3	69.8	φ_2 rotation
ν_{14}	201.7	φ_1 rotation
ν_{64}	864.4	carbazole o.o.p.
ν_{70}	891.0	biphenyl o.o.p.

Table S2 Fluorescence lifetimes and emission quantum yields (Φ) of CBP, measured in various solvents

	Hexane	Ethyl Ether	THF	DCM	MeCN
Lifetime (ns)	1.30	1.78	1.80	1.85	2.59
Φ	0.57	-	-	0.70	0.63

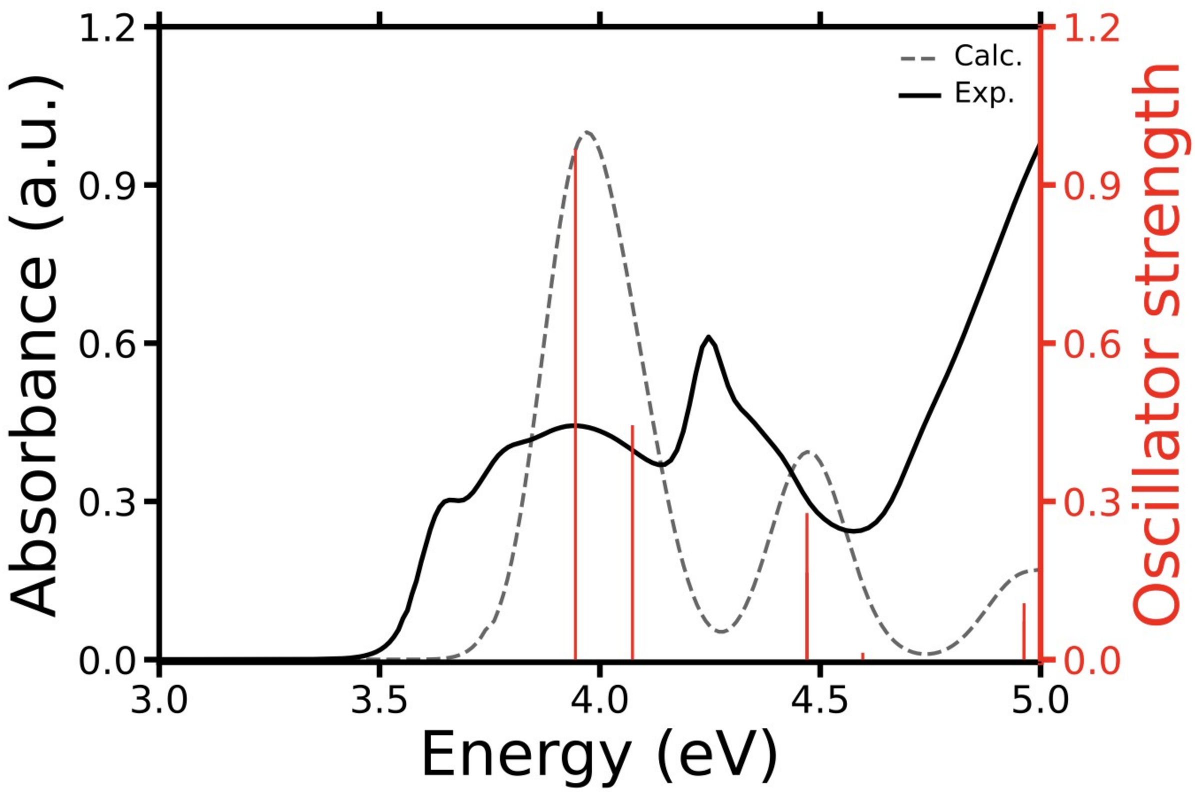

Fig. S1 Comparison of calculated and experimental spectra. Vertical red lines indicate the calculated oscillator strength. The calculated spectra have been red-shifted by 0.5 eV for alignment with experimental spectra.

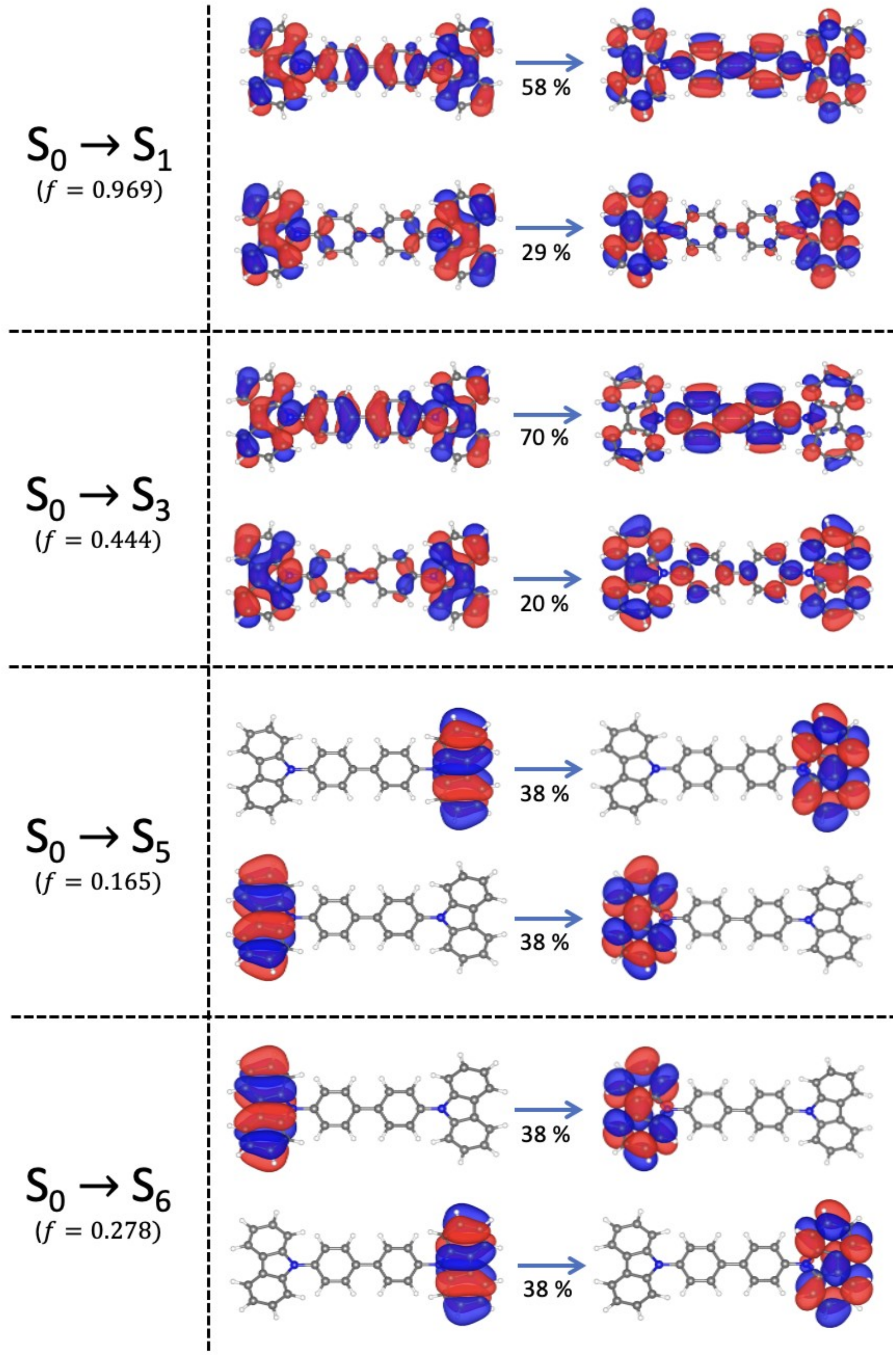

Fig. S2 Natural transition orbitals (NTOs) and associated oscillator strengths corresponding to the bright excited states of CBP.

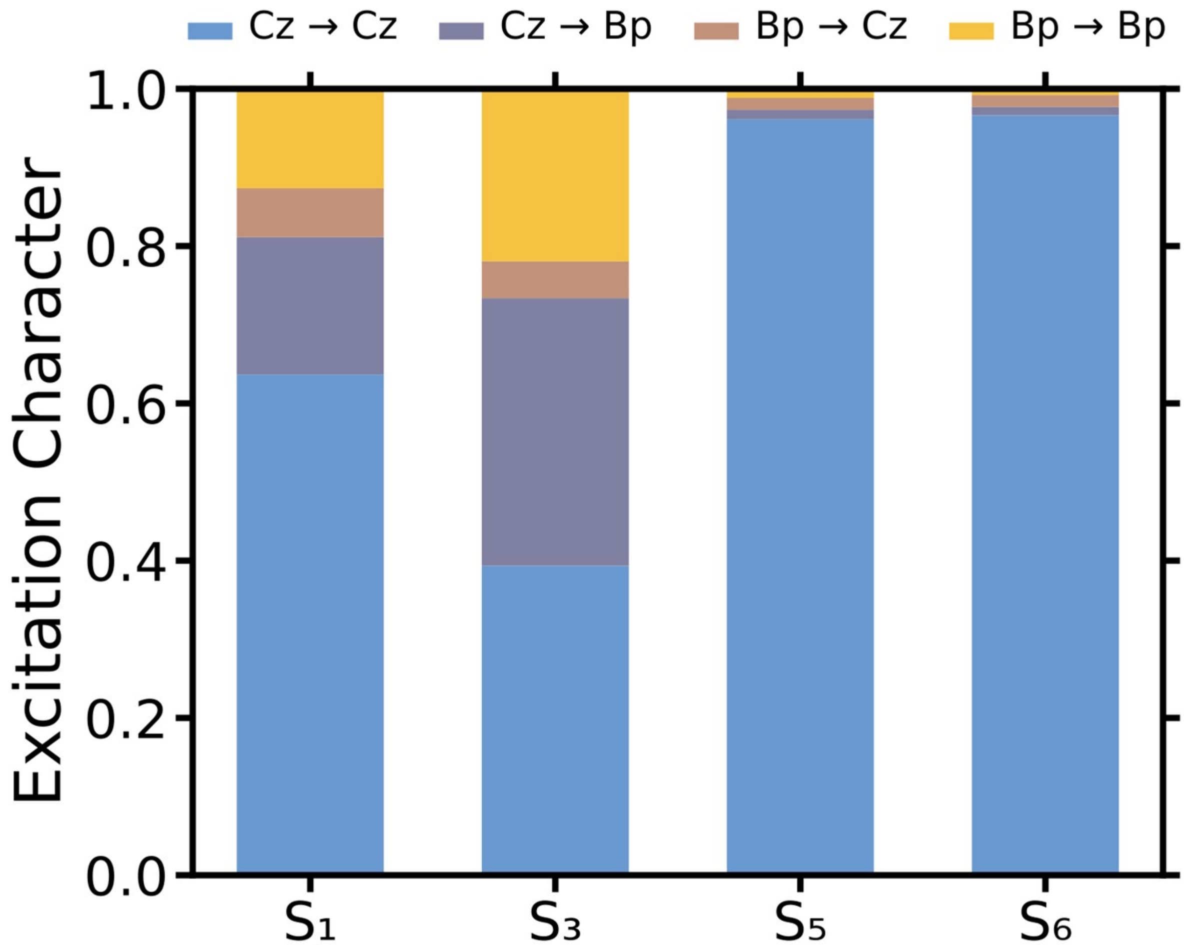

Fig. S3 Excitation character of the two molecular fragments. Employing the 1-TDM analysis, we calculated the excitation character of each fragment. The excitation character between the two fragments was evaluated for the bright excited states. Here, Cz represents the carbazole group, and BP denotes biphenyl.

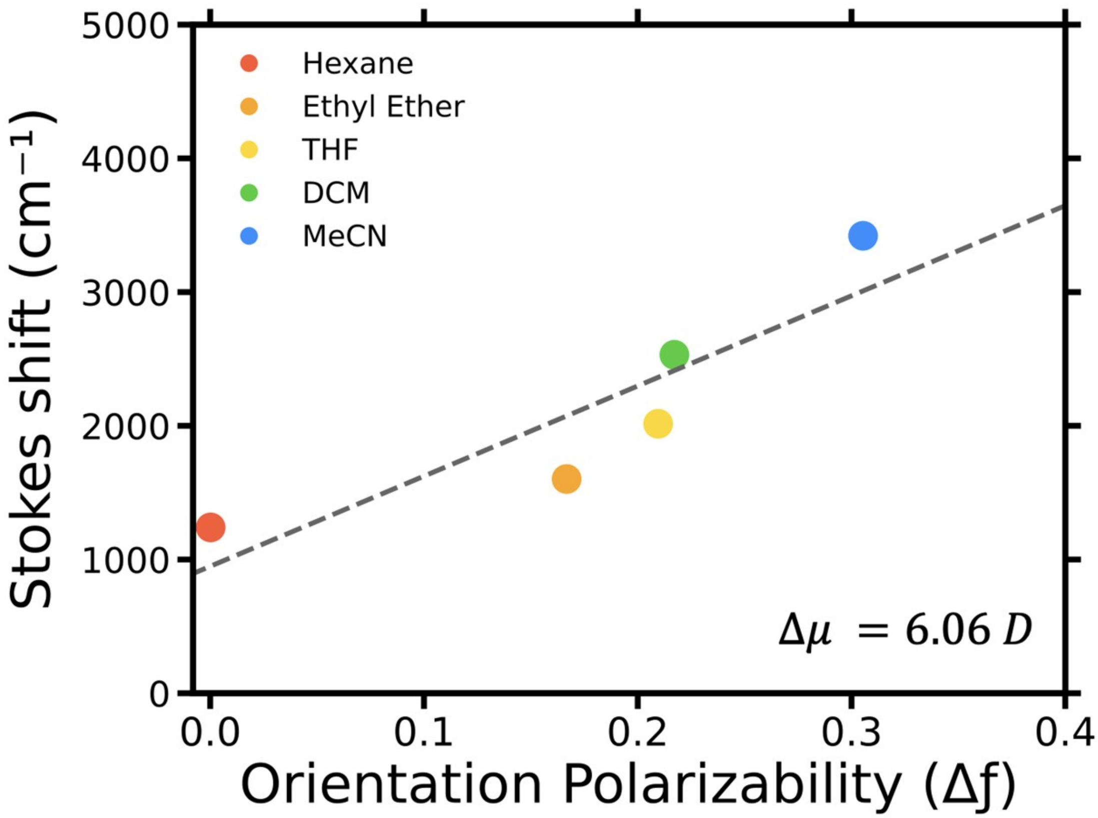

Fig. S4 Lippert-Mataga plot of CBP in various solvent conditions, showing the Stokes shift as a function of orientation polarizability.

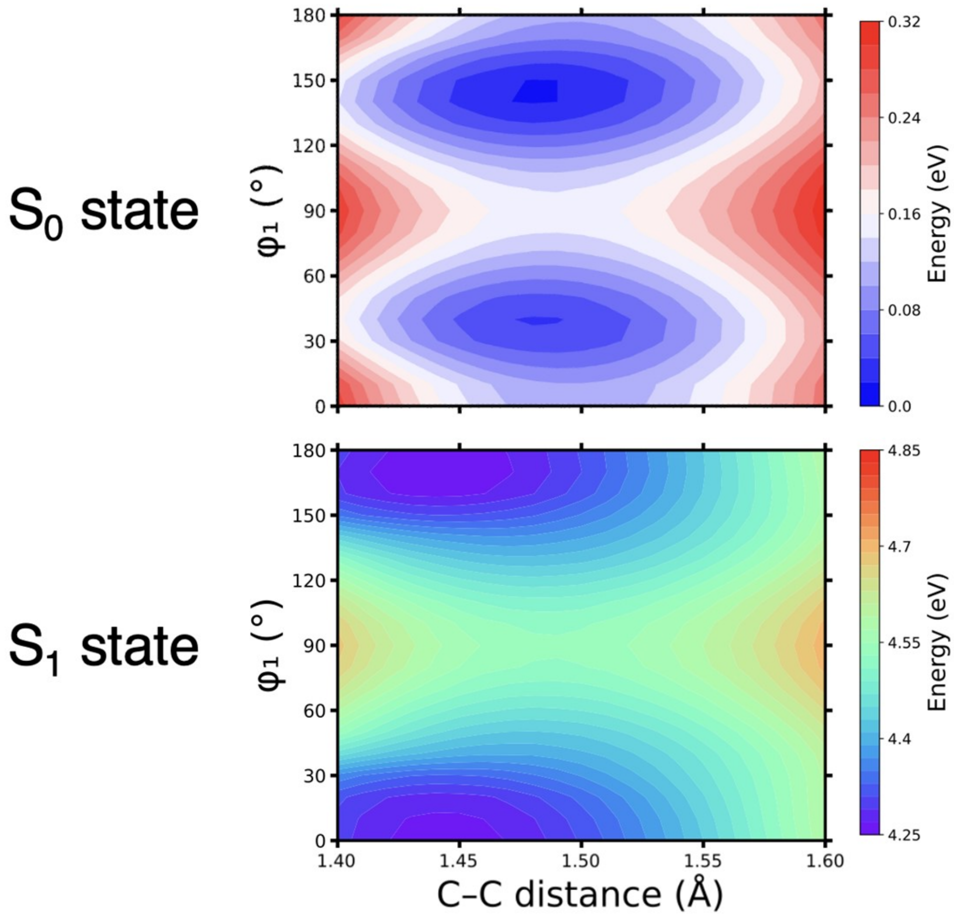

Fig. S5 Two-dimensional potential energy surfaces (PESs) of CBP in the S_0 and S_1 states plotted with respect to the biphenyl torsion angle (φ_1) and the $r_{c\text{-}c}$ between the two phenyl rings in the biphenyl unit.

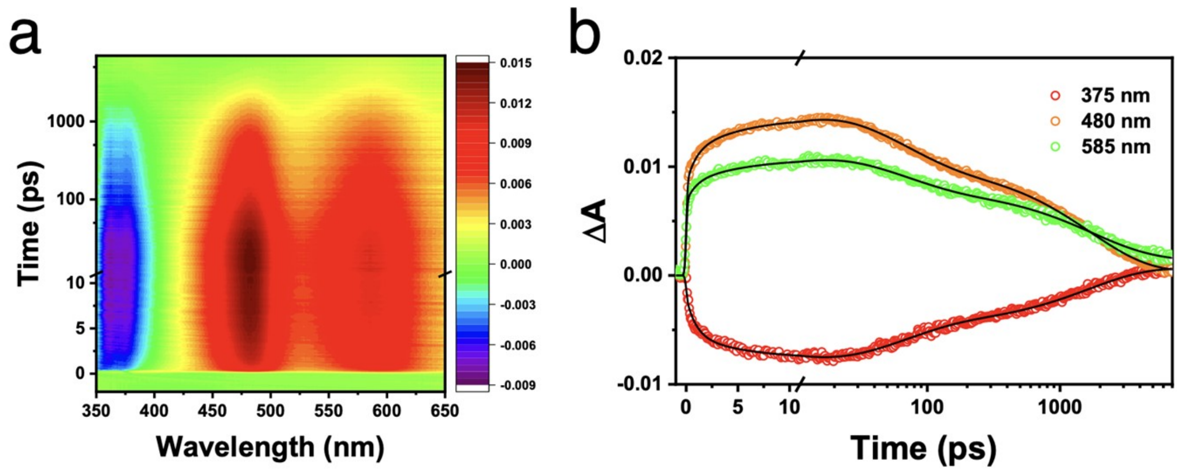

Fig. S6 Time-resolved transient absorption data for CBP in ethyl ether. (a) Contour plots of TA spectra of CBP in ethyl ether. (b) Time profiles monitored at selected wavelengths (red: 375 nm, orange: 480 nm, and green: 585 nm). All decay profiles were well-expressed by a tetra-exponential function (0.97 ± 0.10 ps, 7.8 ± 0.3 ps, 64 ± 1 ps, and 1718 ± 15 ps). Fit curves are shown in black solid lines.

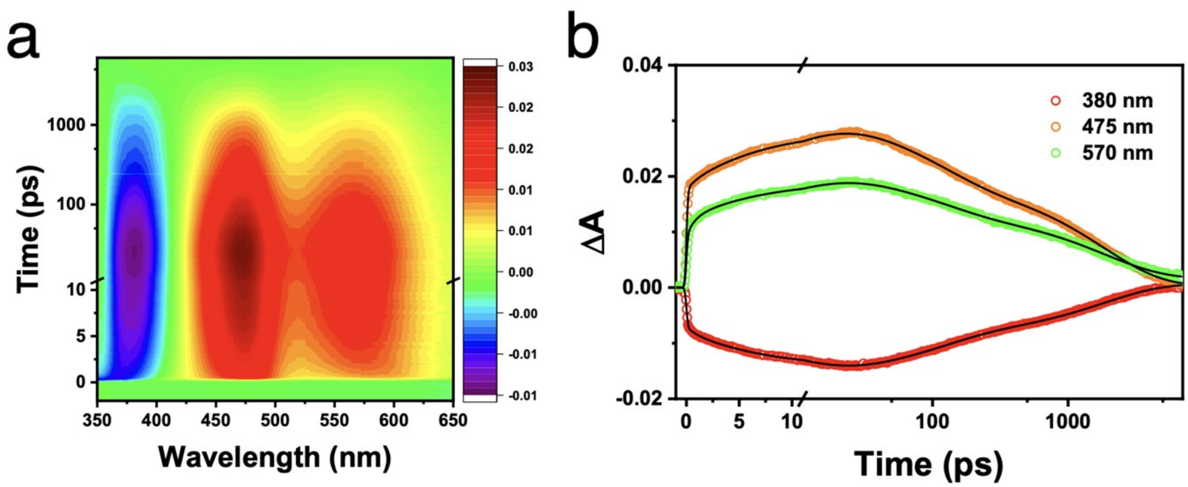

Fig. S7 Time-resolved transient absorption data for CBP in DCM. (a) Contour plots of TA spectra of CBP in DCM. (b) Time profiles monitored at selected wavelengths (red: 380 nm, orange: 475 nm, and green: 570 nm). All decay profiles were well-expressed by a tetra-exponential function (0.75 ± 0.07 ps, 8.9 ± 0.1 ps, 104 ± 1 ps, and 1836 ± 1 ps). Fit curves are shown in black solid lines.

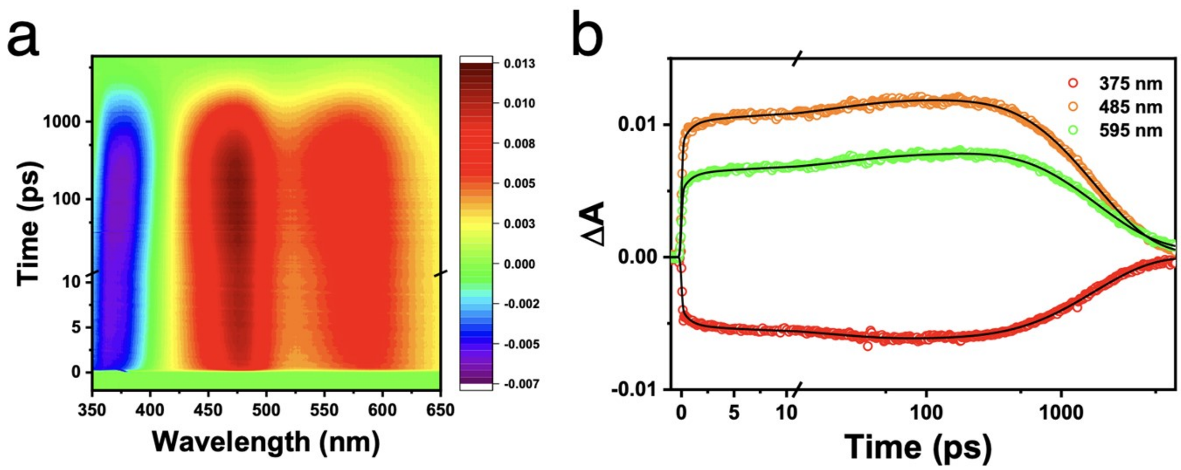

Fig. S8 Time-resolved transient absorption data for CBP in triacetin. (a) Contour plots of TA spectra of CBP in triacetin. (b) Time profiles monitored at selected wavelengths (red: 375 nm, orange: 485 nm, and green: 595 nm). All decay profiles were well-expressed by a tetra-exponential function (0.92 ± 0.05 ps, 20.5 ± 0.9 ps, 241 ± 9 ps, and 1571 ± 15 ps). Fit curves are shown in black solid lines.

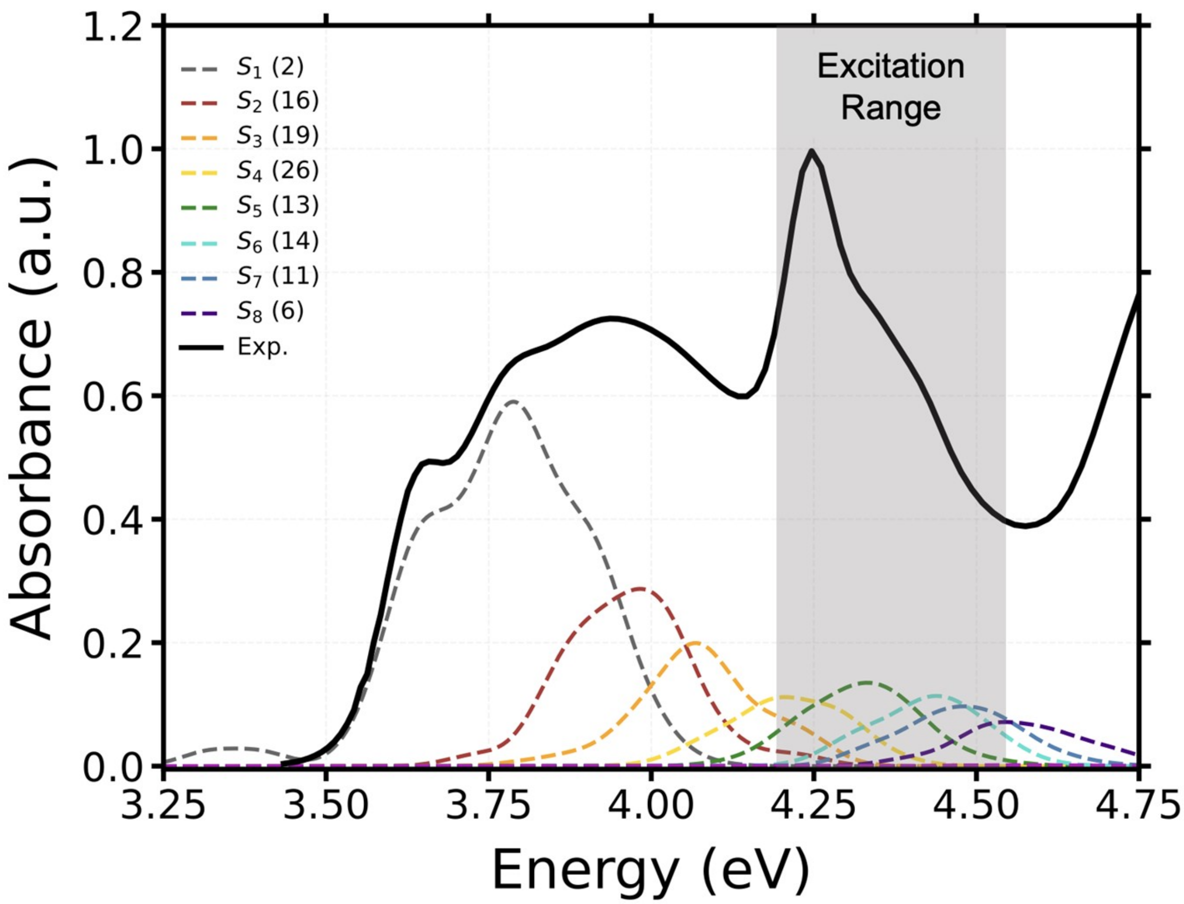

Fig. S9 Calculated absorption cross-section of CBP, derived from 200 geometries sampled using a harmonic Wigner distribution. Based on this absorption cross-section, NAMD simulations were initiated from excited states stochastically selected according to oscillator strength and the chosen excitation range (shaded in grey). The calculated spectra are red shifted by 0.5 eV to align with experimental data. The numbers in parentheses indicate the number of trajectories launched from the corresponding excited state.

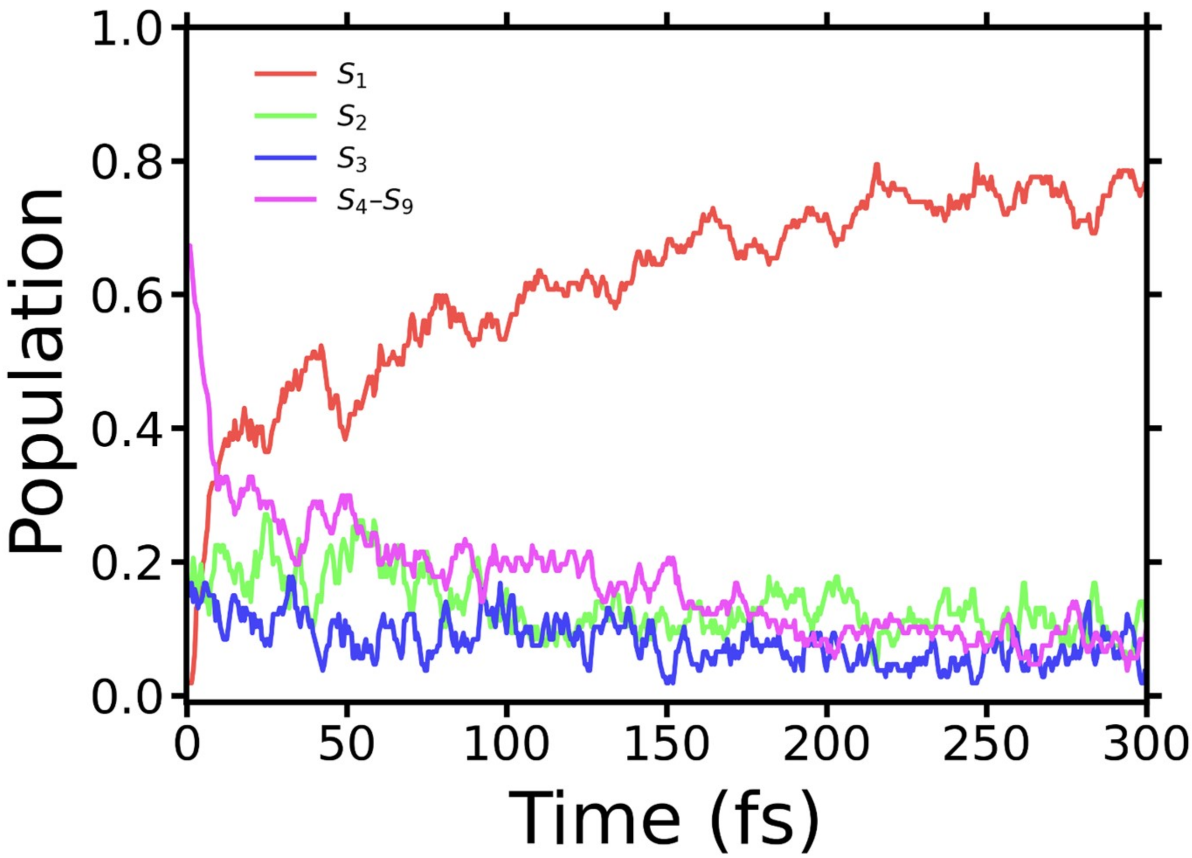

Fig. S10 Time-resolved adiabatic state population of CBP obtained from NAMD simulations.

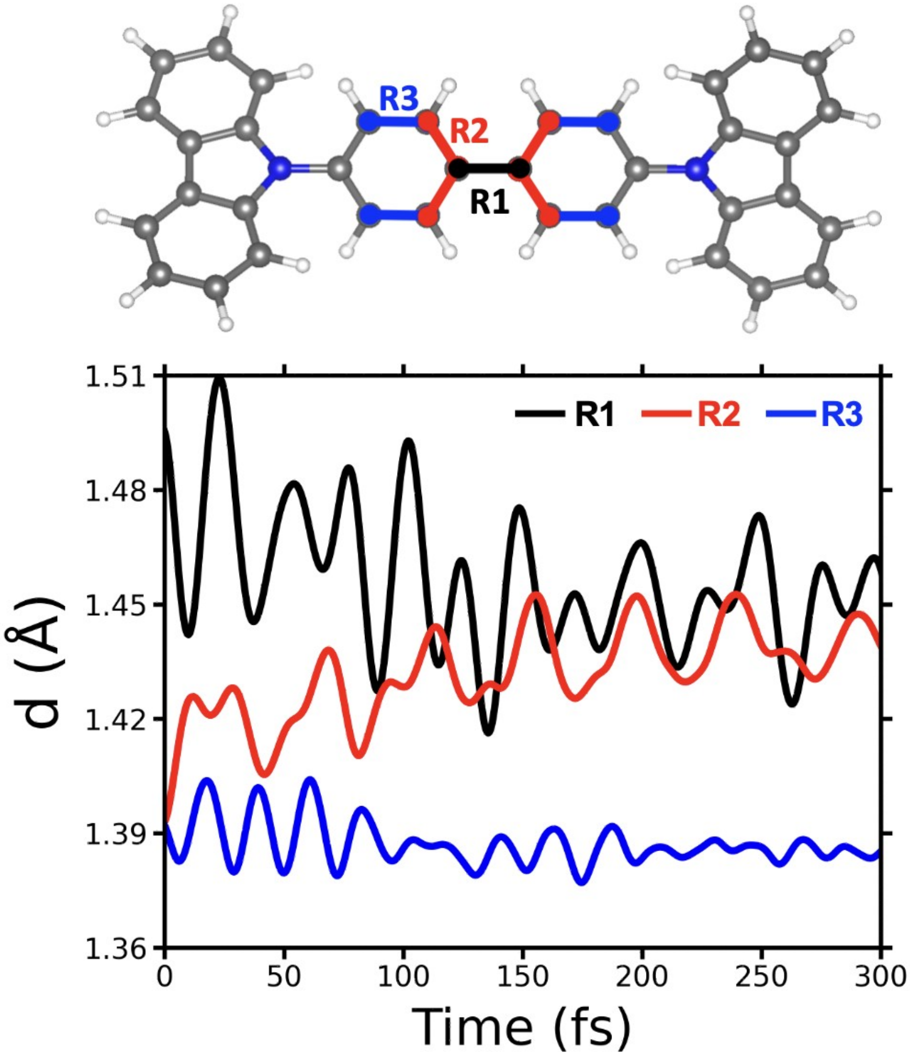

Fig. S11 Time evolution of the averaged C–C bond distances in the biphenyl unit, obtained from the trajectories of NAMD simulations. Considering the molecular symmetry of CBP, the averaged distances are reported for the R2 and R3 positions.

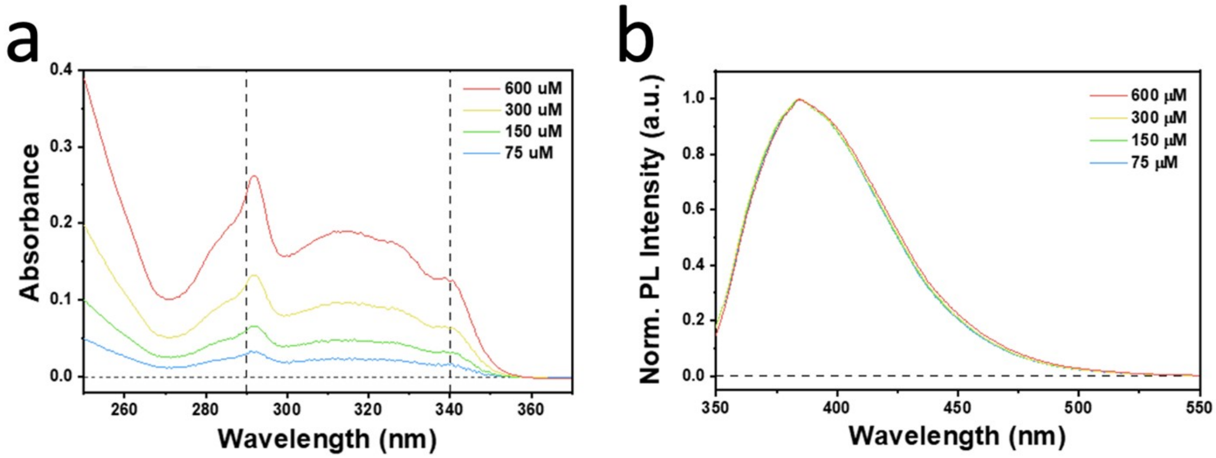

Fig. S12 (a) Absorption spectra and (b) emission spectra of CBP measured at four different concentrations.